

STUB COLUMN TESTS AND FINITE ELEMENT MODELLING OF COLD-ROLLED ALUMINIUM ALLOY 5052 CHANNEL SECTIONS

Le Anh Thi HUYNH^a, Cao Hung PHAM^a and Kim J.R. RASMUSSEN^a

^a School of Civil Engineering, The University of Sydney, NSW 2006, Australia

Emails: leanhthi.huynh@sydney.edu.au, caohung.pham@sydney.edu.au, kim.rasmussen@sydney.edu.au

Keywords: Aluminium alloys; Cold-rolled sections; Section capacity; Stub column tests; Local buckling; Post-buckling; Finite Element Modelling.

Abstract: *Aluminium structural members are usually produced by extrusion. Recently, aluminum Z- and C- sections have been successfully cold-formed from aluminium coil using existing rollers for cold-formed steel sections. This paper presents an experimental program on cold-rolled aluminium C-sections subject to axial load. A total of twelve stub columns were performed at the University of Sydney under compressive loading condition between two fixed end supports. Three different commercially available lipped C-sections with different slenderness were chosen for testing, and subsequently analysed numerically using the Finite Element Method (FEM). The FEM models incorporating measured input parameters such as the material properties and actual initial geometric imperfections are compared with the experimental results. Depending on the slenderness of the sections, it was observed in the experiments that local buckling occurred quite early and that the sections exhibited extensive post-local buckling reserve strength. The behaviour and strengths obtained experimentally and numerically are discussed in this paper.*

1 INTRODUCTION

For many years, cold-formed structural members have dominated in wall and roof systems for industrial and commercial buildings as well as in applications like plane and space trusses, floor bearers and primary structural frames like portal frames. Cold-formed structural members can be used efficiently due to their high strength-to-weight ratio, ease of fabrication and transportation, and simple erection and installation [1]. The majority of cold-formed structures have been made of steel or stainless steel. In parallel, aluminium structures have become more popular providing new solutions to compete with steel. In pure state, aluminium is a relatively soft metal with tensile strength of approximately 90 MPa. However, a substantial increase in strength can be achieved by alloying aluminium with small percentages of other metals and elements such as manganese, silicon, copper, magnesium or zinc. Two major characteristics that give aluminium alloys extreme versatility are light weight combined with strength and high corrosion resistance, of which the latter provides ideal solutions for applications in corrosive environments, such as coastal areas and corrosive industrial sites.

The earliest examples of the use of aluminum alloys in building structures date back to the 1950s [2]. Subsequently, its use has been spread to a wider range of construction applications including building facades, roof systems and structures situated in humid environments. Aluminium structural members also lend themselves for use in green/sustainable buildings.

In Australia, aluminum structural solutions, well-known as PERMALITE[®] [3], consist of aluminum cladding and structural C- and Z-sections. In the past, these C- and Z- sections

were produced by extrusion and were frequently fabricated overseas. However, in recent years, successful trials have been undertaken to cold-roll aluminum coil into C- and Z-sections, as shown in Fig. 1. By using existing rollers for cold-formed steel sections, the trials have demonstrated that it is possible to roll-form aluminum sections to within acceptable dimensional tolerances.



Figure 1: Cold-rolled C- and Z- sections

In current Australian Standards, guidelines for the design of aluminium structures are covered by AS1664.1 [4]. These guidelines are premised on research on extruded sections and do not allow the increase in strength produced by cold-forming to be accounted for. Currently, there are no design guidelines for these types of cold-rolled aluminium structural members. This has opened the door for not only Australian companies but for cold-formed steel/ stainless steel manufacturing companies worldwide to commercialise cold-rolled aluminium structural sections. The main innovation is that the roll-forming is a new way of producing aluminium structural sections, which has the potential to lead to strength enhancement compared to extrusion and is a more cost effective method of production.

As seen in cold-formed steel sections, thin-walled channels may undergo one of three fundamental modes of buckling, viz. local, distortional and lateral-torsional buckling, or combinations of these modes. In this study, thin-walled aluminium stub columns may experience local buckling prior to overall failure of the section. The ultimate load is significantly higher than the load at which the member buckles elastically. Thus, the thin-walled section exhibits substantial post-buckling strength.

This paper presents an experimental program performed at the University of Sydney focusing on the buckling and post-buckling response of cold-rolled aluminium C- section stub columns under compression. Typical sections with slenderness ranging from stocky to slender have been chosen for testing. Also, Finite Element Method (FEM) models have been calibrated against the experimental results and implemented to study the post-buckling behaviour and strength. The comparison of the buckling loads and ultimate loads through experiments and numerical analyses shows good correlation.

2 EXPERIMENTS ON COLD-ROLLED ALUMINIUM CHANNEL SECTION STUB COLUMNS

The experimental program consists of a total of 12 tests conducted in the J.W. Roderick Laboratory for Materials and Structures at the University of Sydney. All tests were performed in the 2000 kN capacity DARTEC testing machine, using a servo-controlled hydraulic ram. All cold-rolled sections were manufactured and supplied by Permalite Ltd (BlueScope), Australia.

2.1 Specimen nomenclature and dimensions

The 12 stub column specimens chosen for the experimental investigation were selected using three commercially available C-sections (C10030, C25025 and C40030) cold-rolled from 5052 aluminum alloy strip. The nominal dimensions are given in Fig. 1 and Table 1. Due to the release of residual stresses at the cut ends, flaring of the cross-sections was observed at the two ends, referred to as Sections A and B in Fig. 2.

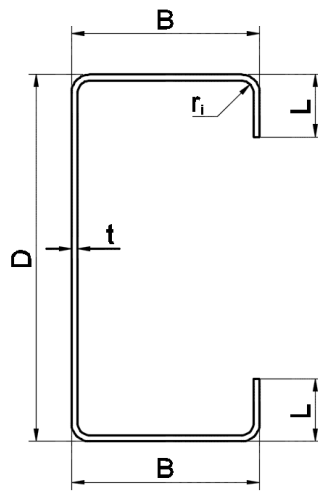


Figure 1. Gross section geometry

Table 1. Nominal dimensions of three sizes of specimens

Specimen	Thickness t mm	Depth D mm	Width B mm	Lip L mm	Inner radius r_i mm
C10030	3.0	105	60.5	16.0	5
C25025	2.5	255	76.0	25.5	6
C40030	3.0	400	125.5	30.0	6

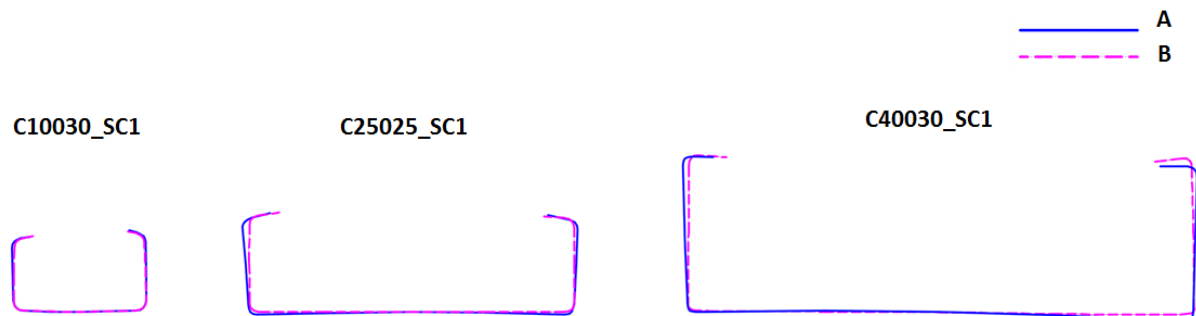


Figure 2: Actual cross-sections at the two ends (Sections A and B)

According to the Guide to Stability Design Criteria for Metal Structures [5], the geometric length (L) of each stub column specimen was taken between $3d$ and $20r$, where d is the depth of the section and r is the least radius of gyration. For the three sections studied, the lengths of the C10030, C25025 and C40030 sections were chosen as 310 mm, 600 mm and 1000 mm, respectively, as shown in Fig. 3.

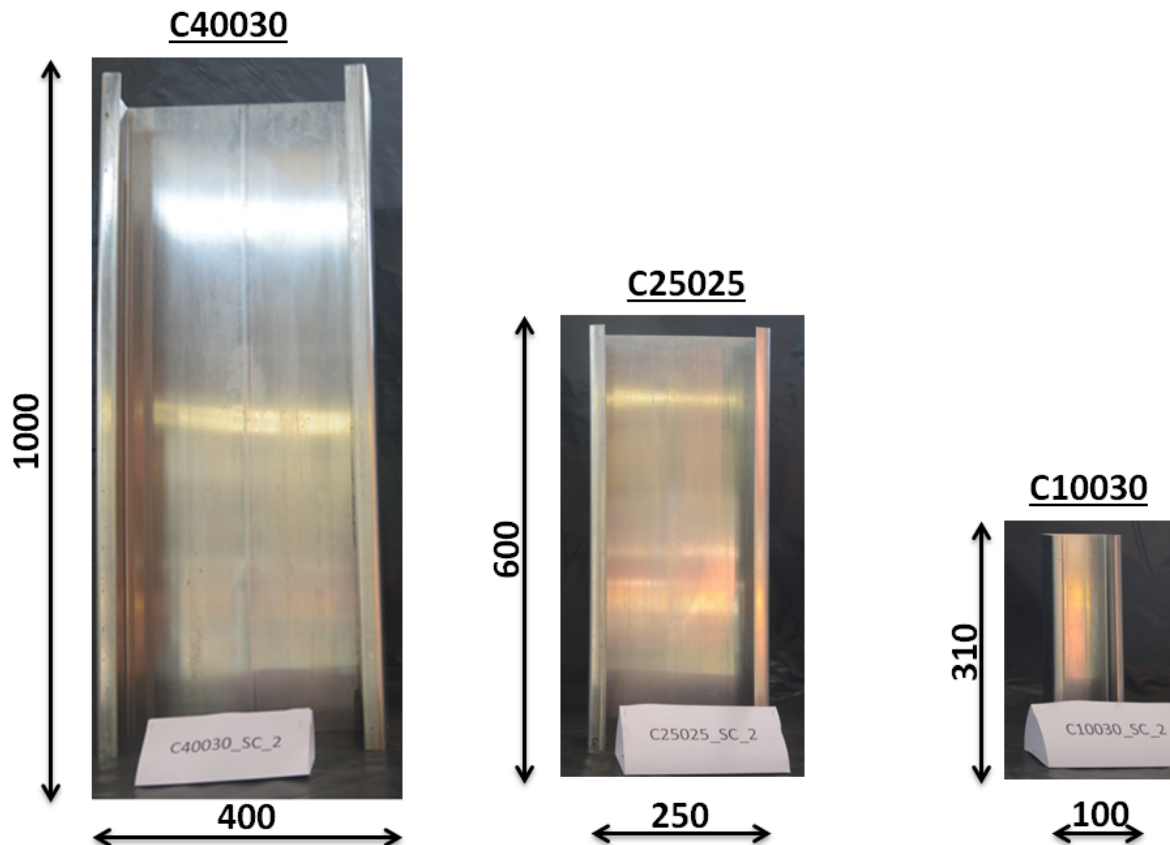


Figure 3: Stub column test specimens

The test specimen was labelled to express the type of channel section, thickness and number of stub column test. For example, the label for a typical test “C10030-SC1” is defined as follows:

- (i) “C100” indicates a C-section with the depth of 100 mm (alternatively “C250” and “C400” for sections with depths of 250 mm and 400 mm respectively).
- (ii) “30” is the nominal thickness 3.0 mm times 10 in mm (alternatively “25” for 2.5 mm).
- (iii) “SC1” indicates Stub Column test number 1.

2.2 Imperfection measurements

Similarly to cold-formed steel structures, initial geometric imperfections have a significant effect on the load carrying capacity of thin-walled aluminium structures. It is therefore necessary to measure the actual initial imperfections prior to testing. The arrangement for the imperfection measurement of each specimen is shown in Fig. 4, in which nine laser measuring devices travel along high-precision tracks while recording the distance to nine corresponding points on the surface of the specimen. The measurement lines are located around the cross-section as also shown in Fig. 4. The laser transducers were programmed to take readings about every 2 mm along the length of the specimen. Each laser transducer had a reading range of approximately 10 mm – 25 mm.

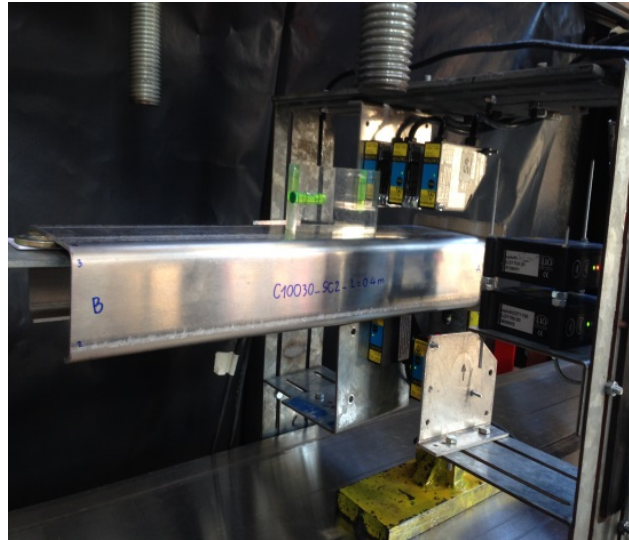
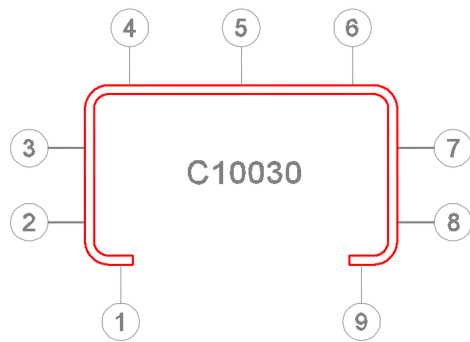


Figure 4: Imperfection measurement lines and imperfection measurement rig

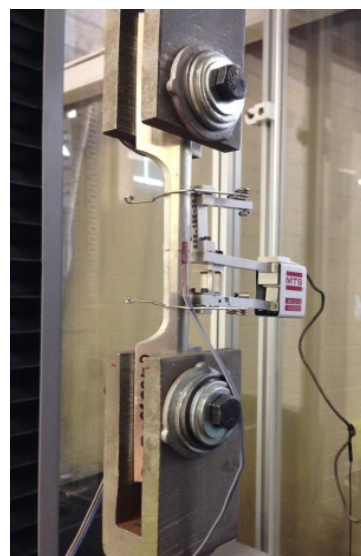
Based on data from the laser readings, the imperfection magnitude values are directly entered into the node numbers for the entire specimen created by the finite element model. The imperfection magnitudes are obtained using a Fourier series approximation longitudinally and linear (for the flanges and lips) or quadratic (for the web) interpolation transversely.

2.3 Material properties

In order to determine the mechanical properties of the cold-rolled 5052 aluminium alloy sections used for the stub column tests, both flat and corner coupons were taken longitudinally from the flat portions and the corners of the sections respectively. The flat coupon dimensions conformed to the Australian Standard AS 1391:2007 [6] for the tensile testing of metals using 12.5 mm wide coupons and a gauge length of 50 mm. The corner coupons were tested between two pins using purpose-built mounts, as shown Fig. 5.



a. Flat coupon test



b. Corner coupon test

Figure 5: Tensile coupon test configurations

The coupons were tested in a 50 kN capacity MTS Model 43 testing machine operated in displacement control mode. In a typical test, a displacement rate of 0.4 mm/min (corresponding to a strain rate of about 2.5×10^{-4} /s) was used. The calibrated extensometer of 50 mm gauge length attached at the middle of the coupon was used to measure the longitudinal strain for the flat coupons. In addition, for corner coupons, two linear strain gauges were attached at the center of each face of the coupon. The strain gauge readings were used to determine the initial Young's modulus. A data acquisition system was used to record the load and readings of strain at regular intervals during the tests. The static load was obtained by pausing the extension for approximately 2 minutes at the 0.2% proof stress and at the ultimate tensile strength. This allowed for the complete static stress-strain curve to be determined.

The average material properties are summarized in Table 2, where the symbols are defined as follows: E_o is the initial Young's modulus, $\sigma_{0.2}$ is the static 0.2% proof stress, σ_u is the material ultimate tensile strength, ϵ_f the plastic strain at fracture, measured over a gauge length of 50 mm, and n is the exponent of the standard Ramberg-Osgood expression [7], obtained using $n = \ln(\epsilon_{0.01}/\epsilon_{0.2}) / \ln(\sigma_{0.01}/\sigma_{0.2})$. Further details about the coupon tests are provided in the companion paper in this conference [8].

Table 2: Material properties obtained from tensile coupon tests

Coupon	Position	$\sigma_{0.2}$ MPa	σ_u MPa	E_o GPa	ϵ_f %	n
C10030	flat	220	267	69.3	4.4	12.0
C25025	flat	215	262	69.7	4.8	12.8
C40030	flat	220	268	69.9	5.2	13.5
C10030	corner	244	290	70.1	7.3	15.8
C25025	corner	248	292	71.2	8.6	16.4
C40030	corner	240	282	70.5	7.0	18.1

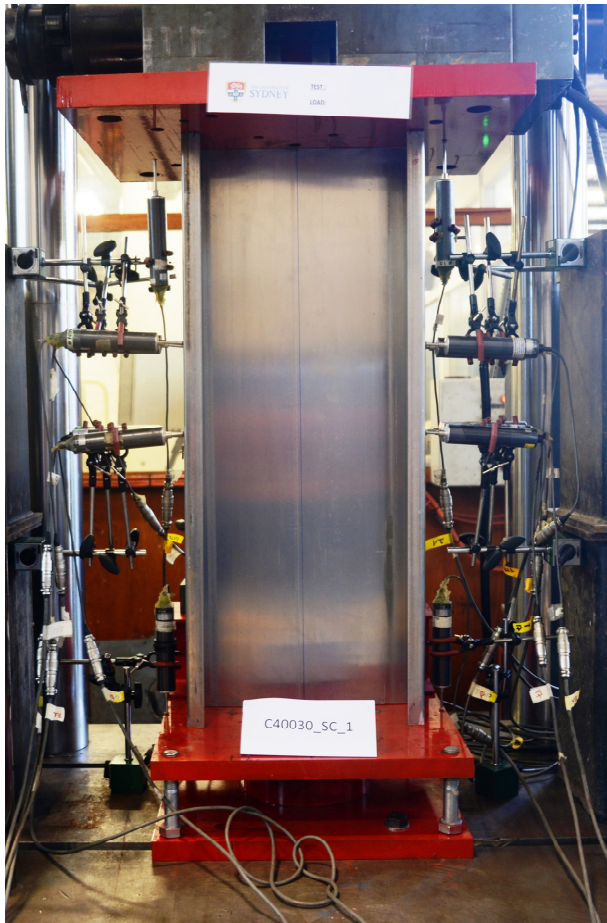
3 COLD-ROLLED ALUMINIUM STUB COLUMN TESTS

3.1 Test set-up and experimental results

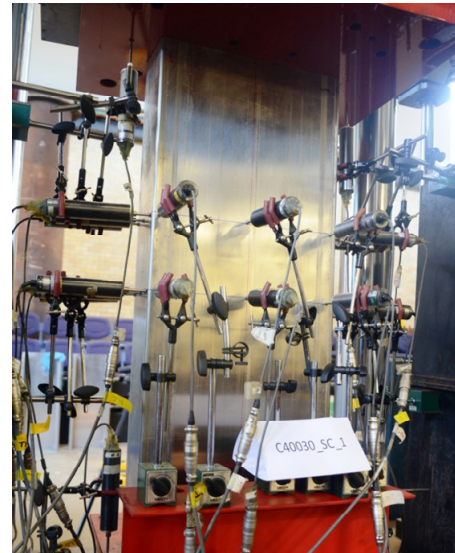
The cold-rolled aluminium stub column tests were performed in a 2000 kN capacity DARTEC displacement controlled hydraulic testing machine. The test specimen was placed vertically between two fixed ends. A diagram of the test set-up configuration is shown in Fig. 6a. At the top end, a square steel bearing plate of 40 mm thickness was attached to the DARTEC loading ram. At the bottom end, the base consisted of two bearing plates of 32 mm thickness connected by a spherical head as shown in detail in Fig. 6c. Initially, the DARTEC loading ram was moved slowly downwards to apply a very small load to the section. This caused the spherical head to rotate slightly until full contact between the end plate and the specimen was achieved, thus ensuring the load was applied uniformly across the entire section. Four bolts installed at the four corners of the two bearing plates were subsequently adjusted to lock the two plates into a fixed position, as also seen in Fig. 6c. The set-up ensured that initially, the load was applied concentrically between two fixed ends as per the guidelines of the Structural Stability Research Council [5].

Once the bearing at the bottom was locked against rotation, the DARTEC loading ram was programmed to move downwards at a constant stroke rate of 0.5 mm/min throughout the test

and well into the post-ultimate range. For each section size, four nominally identical tests were conducted to obtain a measure of the variance in ultimate load and load-displacement response.



a. Front view



b. Back view



c. Base detail

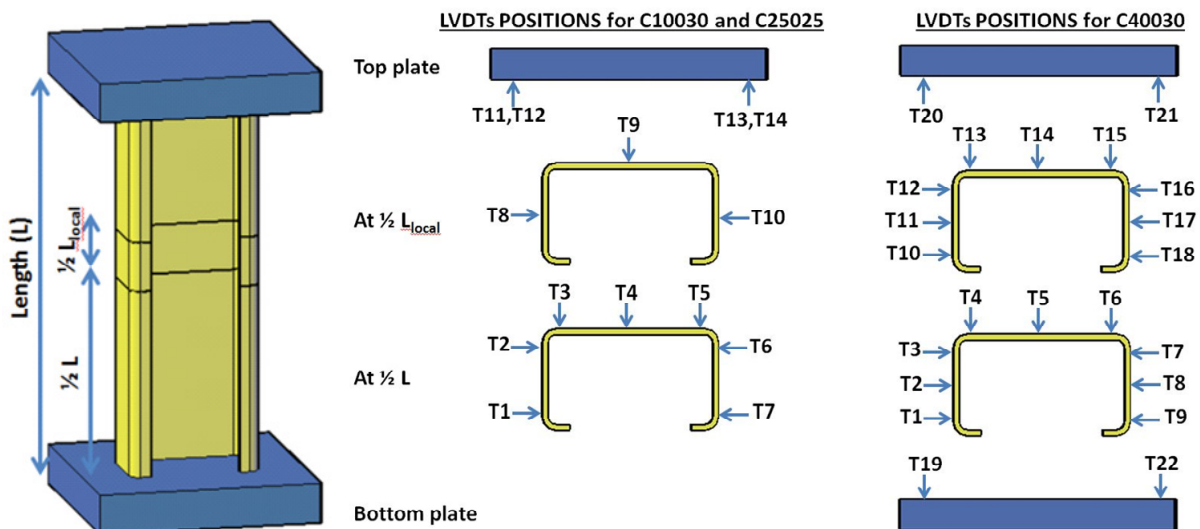


Figure 6: Test set-up for cold-rolled aluminium stub column tests

Four LVDTs (Linear Variable Differential Transformers) were used to measure the vertical displacement. For out-of-plane measurements, 14 to 22 LVDTs were installed symmetrically at the locations shown in Fig. 6. All LVDTs were mounted directly to the base of the DARTEC testing machine. This setup allowed for the vertical displacement of the specimen to be determined without being affected by the distortion of the test specimen. Each LVDT was calibrated and checked prior to performing each test. Data were recorded continuously during the test using a Spectra Data Recording System.

Fig. 7 shows the load-end shortening curves of representative tests for the three cross-sections (C10030, C25025 and C40030). Fig. 8 shows corresponding post-peak failure mode shapes of typical C10030, C25025 and C40030 tests.

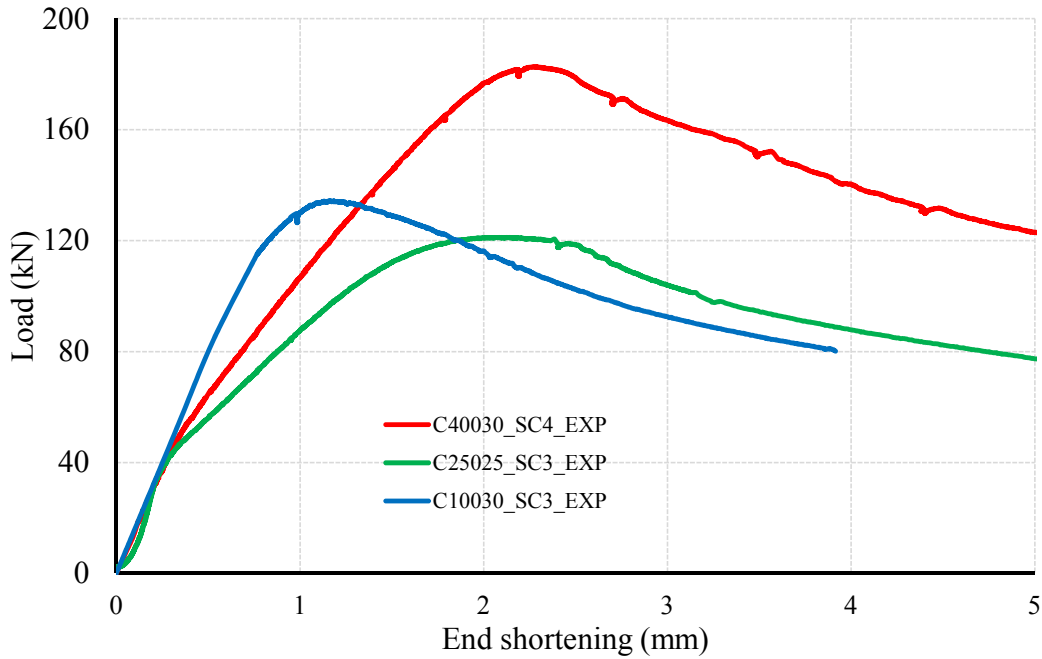


Figure 7: Load vs end shortening curves

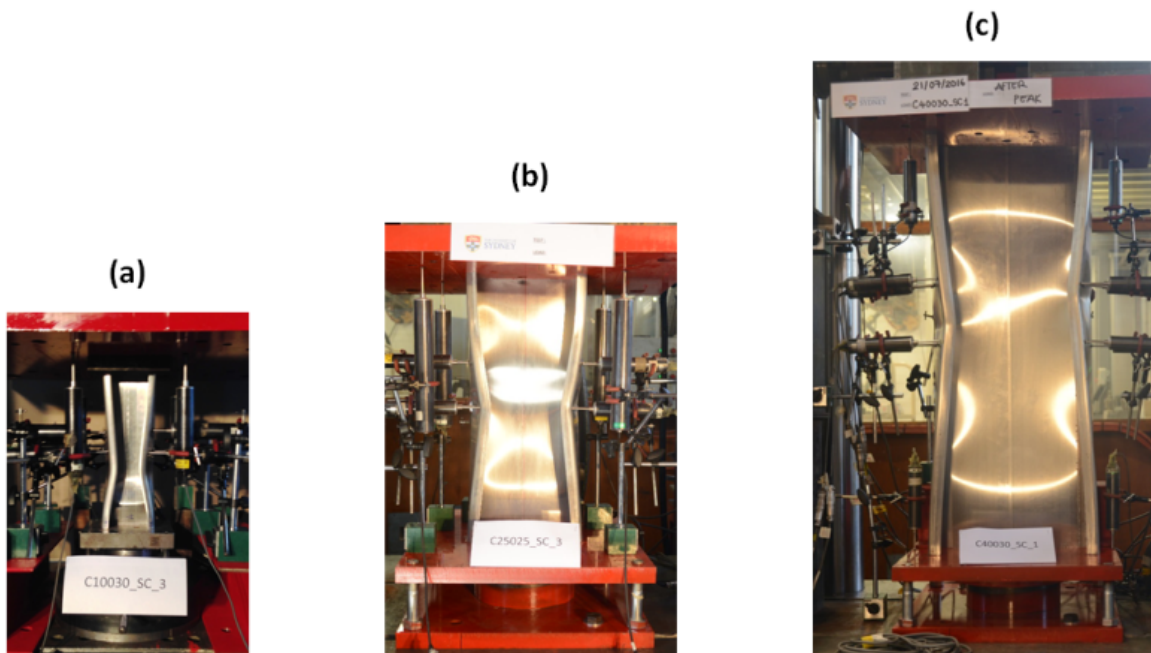


Figure 8: Post-peak failure mode shapes of typical C10030, C25025 and C40030 tests

3.2 Numerical simulation and calibration against test results

The Finite Element Method (FEM) can be used to undertake a geometrically and materially nonlinear inelastic analysis (GMNIA). Detailed Finite Element Method (FEM) models were developed using the commercially available software package ABAQUS/Standard - Version 6.14 [9] to study the behaviour of cold-rolled aluminium channel stub columns under compression. The models were analysed using geometrically and materially nonlinear analyses with imperfections (GMNIA).

In order to obtain realistic results from the finite element nonlinear analyses, plastic strains were included in the material definition. The measured stress-strain curves based on the flat portion and corner coupons tests described in Section 2.3 were included in the model. In the plastic analysis, the static engineering stress-strain curves obtained from tensile coupon tests were converted to true stress *vs* logarithmic true plastic strain curves. The true stress σ_{true} and true plastic strain ϵ_{true} were calculated using equations (1) and (2) as follows:

$$\sigma_{true} = \sigma(1 + \epsilon) \tag{1}$$

$$\epsilon_{true} = \ln(1 + \epsilon) - \frac{\sigma_{true}}{E} \tag{2}$$

where σ and ϵ are the measured engineering stress and strain respectively obtained from the tensile coupon tests. A schematic view of the FEM model is shown in Fig. 9.

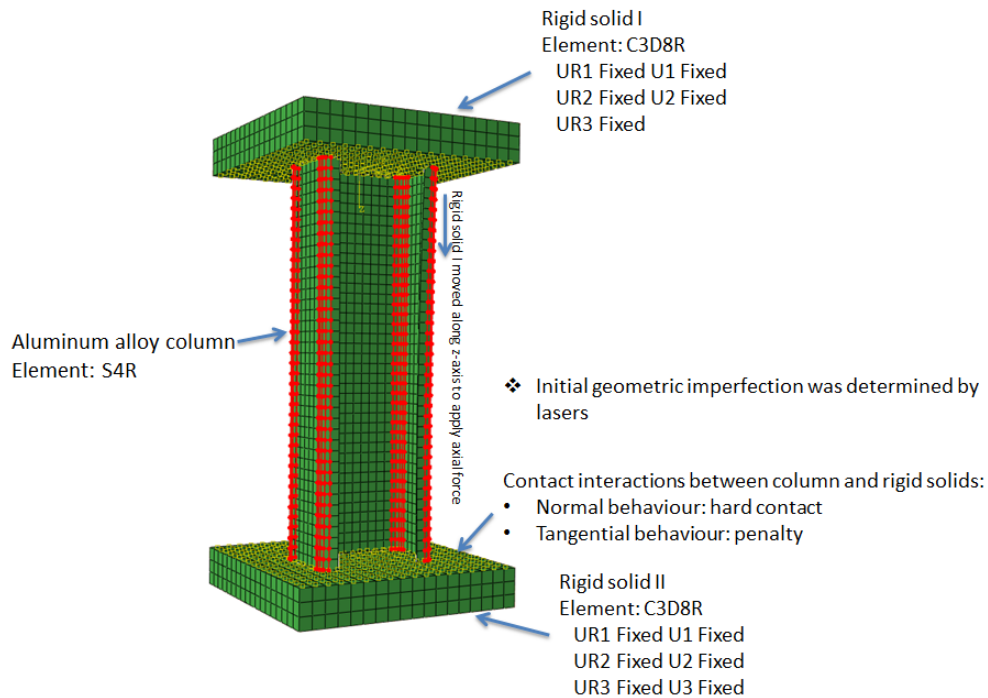


Figure 9: FEM model of cold-rolled aluminium stub column test

The aluminium cold-rolled channels were modelled using the 4-node shell element with reduced integration, type S4R, available from the ABAQUS element library. This shell element uses three translational and three rotational degrees of freedom at each node. The element accounts for finite membrane strains and arbitrarily large rotations. Therefore, it is suitable for large strain analyses and geometrically nonlinear problems. The top and bottom plates at the two ends were generated in ABAQUS using 3D-deformable solid elements and were assigned standard steel properties. Contact between nodes of the cross-section ends

(Sections A and B shown in Fig. 2) and the surfaces of the top and bottom bearing plates was incorporated to obtain realistic failure modes.

The simulation consisted of two steps. In the first step, the measured imperfections were incorporated into the models as follows: (i) the “perfect” model was created in ABAQUS by extruding the actual flared Section A (see Fig. 2); (ii) the out-of-plane initial deformations of the plate elements at the nine measurement lines (see Fig. 4) were then superimposed onto the perfect mesh using a Fourier transformation on the laser reading data points to obtain a representative mathematical expression for the lines of imperfection; (iii) for the remaining nodes between the points along the measurement lines, linear interpolation was used for flanges while quadratic interpolation was used for the web. The second step was a geometric and material nonlinear analysis using the modified RIKS method [10, 11]. Table 3 summarises the ultimate strength results for the 12 stub column tests on cold-rolled aluminium channel sections. Also included in Table 3 are the FEM predictions of the maximum loads and the ratio P_{EXP}/P_{FE} between the experimental and numerical ultimate loads. The mean and coefficient of variation (CoV) of the ratio P_{EXP}/P_{FE} are 0.975 and 0.023 respectively, and the maximum discrepancy is 6%, thus indicating overall good agreement between the experimental and numerical results.

Table 3: Tests and ABAQUS-FEM results

Specimen	Length (mm)	Test		ABAQUS-FEM		$\frac{P_{EXP}}{P_{FE}}$
		P_{EXP} (kN)	Flange movement	P_{FE} (kN)	Flange movement	
C10030_SC1	310	130.9	inward	138.6	inward	0.944
C10030_SC2	310	136.6	inward	140.1	inward	0.975
C10030_SC3	310	134.3	inward	139.0	inward	0.966
C10030_SC4	310	137.0	inward	137.2	inward	0.999
C25025_SC1	600	119.6	inward	118.7	inward	1.007
C25025_SC2	600	116.0	inward	119.6	inward	0.970
C25025_SC3	600	121.2	inward	119.9	inward	1.010
C25025_SC4	600	118.2	inward	125.2	inward	0.944
C40030_SC1	1000	172.1	inward	177.4	inward	0.970
C40030_SC2	1000	170.1	outward	172.1	outward	0.988
C40030_SC3	1000	176.8	inward	186.4	inward	0.949
C40030_SC4	1000	182.7	outward	186.1	outward	0.982
					Mean	0.975
					CoV	0.023

The load-end shortening curves for the C40030-SC4 test (—) and the ABAQUS results without geometric imperfections (---) and with geometric imperfections (—○—) are illustrated in Fig. 10. Excellent agreement between the predicted FE curve with actual initial imperfections and the experimentally recorded curve was obtained. Figs. 11 and 12 compare the predicted lateral displacements of the FE model with the experimentally recorded values. The displacements derived from the FE model were obtained from the nodes corresponding to the locations of LVDTs T1 and T5 (see Fig. 6) in the test. Again, good agreement between the predicted and recorded displacements is observed when the measured imperfections are modelled. Fig. 13 shows observed deformations at the local buckling load, peak load and in the post-peak range.

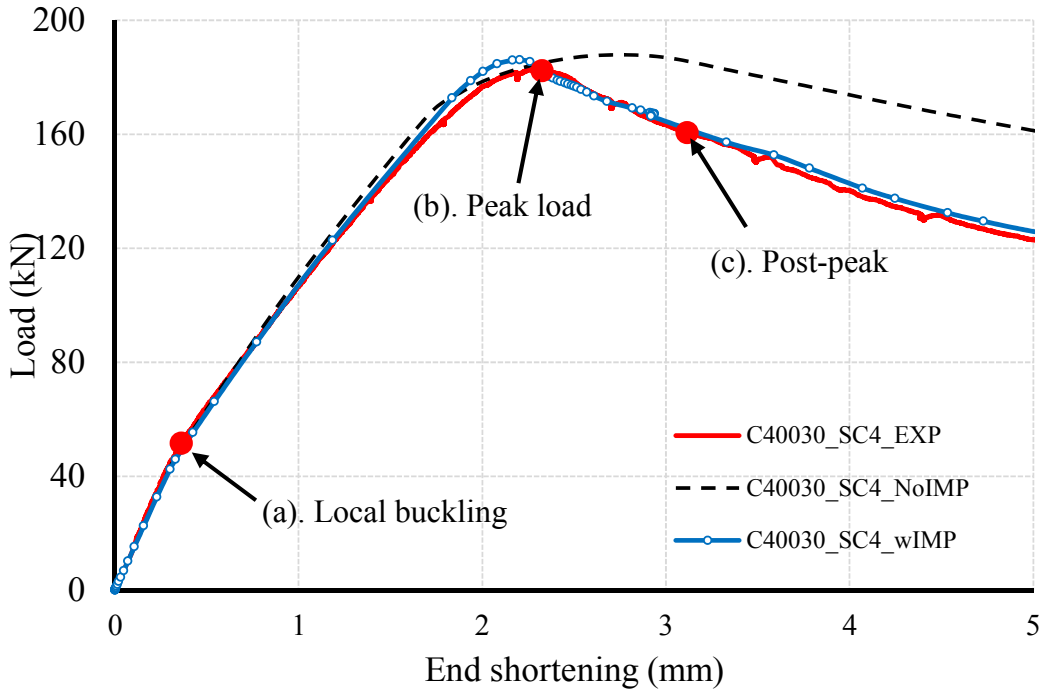


Figure 10: Load vs end shortening relationship for C40030 (Test and FEM)

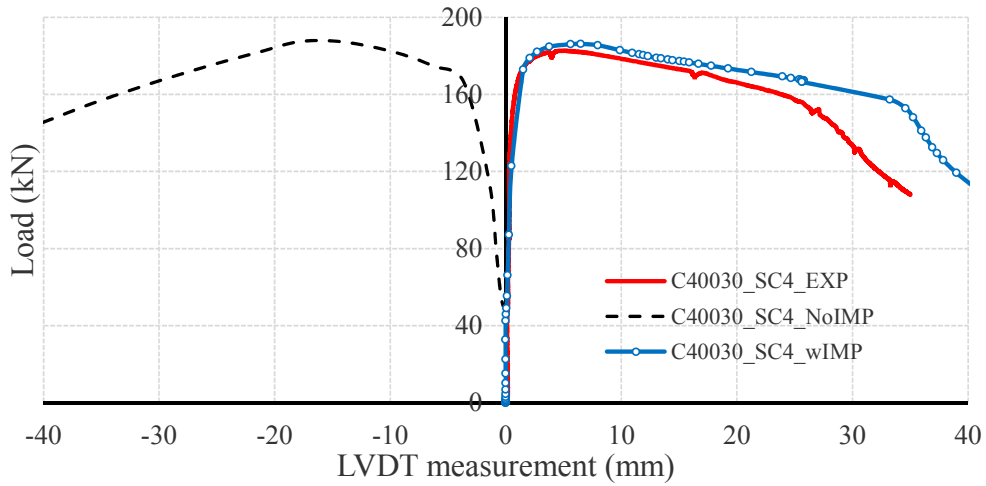


Figure 11: Axial load vs lateral displacement LVDT (T1)

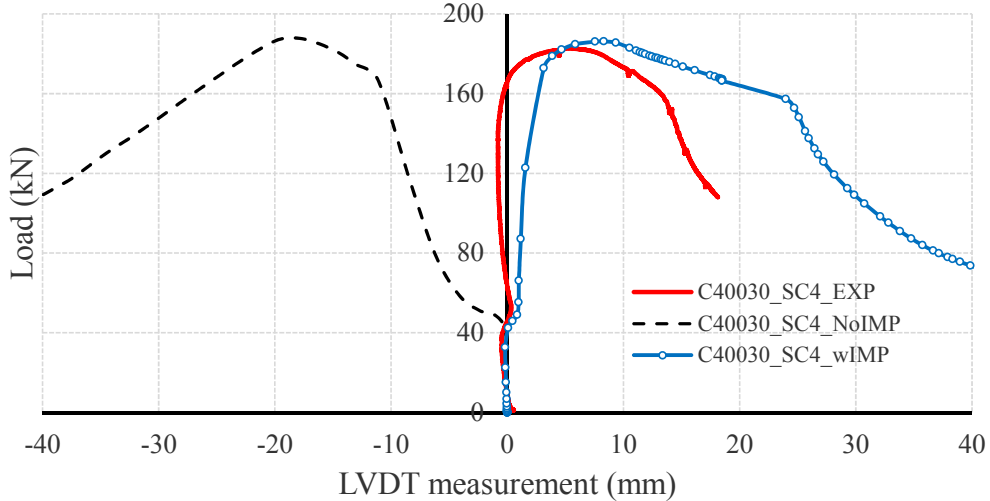
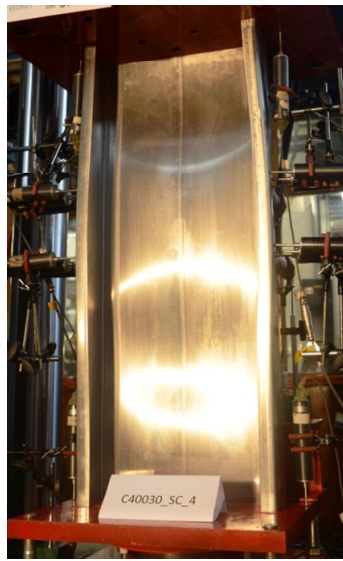


Figure 12: Axial load vs lateral displacement LVDT (T5)



(a). At local buckling

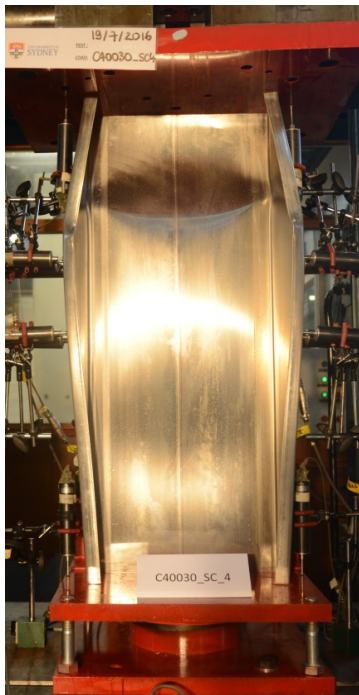


(b). At peak load

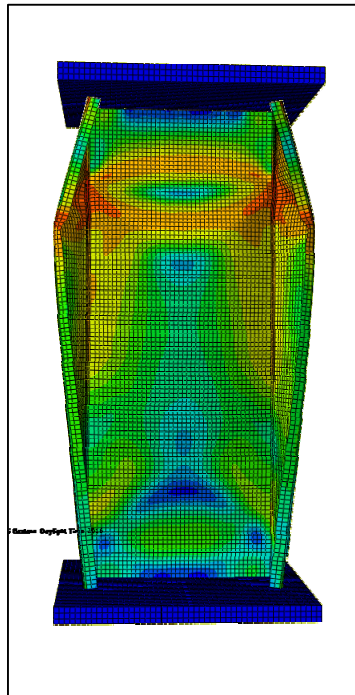


(c). At post-peak

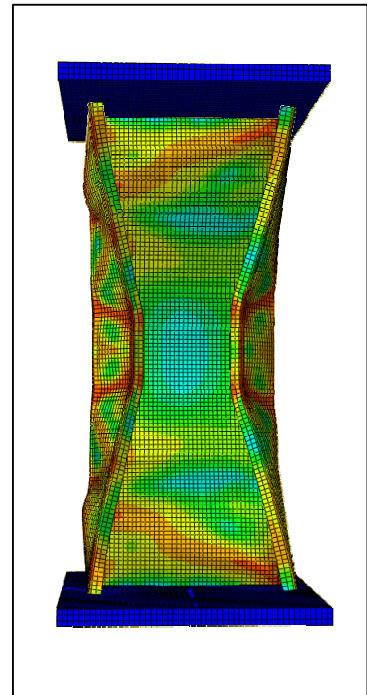
Figure 13: Observed deformations at the local buckling load, peak load and in the post-peak range



(a). At post-peak
(Experiment)



(b). At post-peak
(FEM with Imperfection)



(c). At post-peak
(FEM without Imperfection)

Figure 14: Post-peak failure mode shapes in test and FEM simulations with and without imperfections

As seen in Fig. 10, the load increases nearly linearly up to about 45 kN where local buckling occurs mainly in the web (see buckling mode shape in Fig. 13a and lateral web displacement at LVDT T5 in Fig. 12). The junctions between the lips and flanges remain essentially straight as there is no discernible movement of the flanges as shown in Fig. 13a and Fig. 11. After local buckling, the load continues to increase while the axial stiffness decreases, as indicated by the decreasing slope of the load-end shortening curve up to the peak load (182.7 kN). The failure mode shape at the peak load can be observed in Fig. 13b. The fact that the peak load is four times the local buckling load indicates a significant post-local buckling reserve strength.

Further, the FEM peak loads with and without initial geometric imperfections are 186.1 kN and 187.7 kN respectively which are within 3% of the ultimate load obtained in the test (182.7 kN). Both peak loads are therefore well predicted by the ABAQUS model. The FE results show that, for this quite slender section (C400030), the presence of initial geometric imperfections does not significantly affect the ultimate strength. However, imperfections may affect the direction of the lateral displacements, see Fig. 11 and Fig. 12, and the rate at which local buckling deformations develop.

After the peak, as shown in Fig. 10, the curves of the test and FE prediction with imperfection match well and drop more significantly as compared with that of the FE model without imperfection. The explanation for this result can be seen in Fig. 14 showing the post-peak failure mode shapes observed in the test (Fig. 14a), and obtained from the FE model with imperfection (Fig. 14b) and FE model without imperfection (Fig. 14c). It is evident that in the post-peak range, the flange and lip junctions move outward in the test and in the FE prediction with imperfections (Figs. 14a and 14b), while the junctions move inward (Fig. 14c) in the FE model prediction without imperfections.

5 CONCLUSIONS

This paper has presented a series of twelve stub column tests on cold-rolled aluminium channel sections carried out at the University of Sydney. Three different commercially available lipped C-sections with various slenderness were selected for testing. Numerical modelling (Finite Element Method) using the commercially available software package ABAQUS/Standard was performed. The FEM models were created based on measured material properties and measured initial geometric imperfections. The FEM ultimate strengths and load-displacement curves were shown to be in good agreement with the experimental results. It was observed in the experiments that, for slender sections, local buckling occurred quite early followed by an extensive post-local buckling range. Also, after the peak load, the buckling mode shape could occur in both inward and outward deflection modes depending on the initial geometric imperfections. Research is ongoing at the University of Sydney on developing design guidelines for cold-rolled aluminium sections.

ACKNOWLEDGMENT

Funding provided by the Australian Research Council Linkage Research Grant LP140100563 between BlueScope Lysaght and the University of Sydney has been used to perform this research. The authors would like to thank Permalite Aluminum Building Solutions Pty Ltd for the supply of the test specimens and financial support for the project.

REFERENCES

- [1] G.J. Hancock, Cold-formed steel structures (To Australian/New Zealand Standard AS/NZS 4600:2005), Fourth Ed., 2007.
- [2] F.M. Mazzolani, Aluminium alloy structures, 2nd edition. Chapman & Hall, 1995.
- [3] Permalite Aluminium Building Solutions Pty Ltd, <https://permalite.com.au/>.
- [4] AS/NZS1664.1:1997, Australian / New Zealand Standard Part 1 : Limit state design aluminium structures, Standards Australia, Sydney, 1997.
- [5] R.D. Ziemian, Guide to Stability Design Criteria for Metal Structures, 6th edition, New York, NY John Wiley & Sons, 2010.
- [6] AS 1391:2007, Metallic materials - Tensile testing at ambient temperature, Standards Australia, Sydney, 2007.
- [7] W. Ramberg, W.R. Osgood, Description of stress-strain curves by three parameters, Natl. Advis. Comm. Aeronaut. (NACA), Washington D.C. Technical Note No. 902, 1943.
- [8] L.A.T Huynh, C.H. Pham, and K.J.R. Rasmussen, Mechanical properties of cold-rolled aluminium alloy 5052 channel sections, Proceedings, 8th International Conference on Steel and Aluminium Structures, The University of Hong Kong, Hong Kong, 2016.
- [9] ABAQUS/Standard “ABAQUS/CAE User’s Manual” Dassault Systemes Simulia Corp, Providence, RI, USA. 2014.
- [10] Riks E. The application of Newton's method to the problem of elastic stability. Journal of Applied Mechanics 1972; 39:1060-6.
- [11] Riks E. An incremental approach to the solution of snapping and buckling problems. International Journal of Solids Structures 1979; 15:529-51.